An investigation on the correlation between rabbit femur bone with second order texture properties from Gray Level Co-occurrence Matrix

Resmi S.L[1], P.N Dileep [2]
[1]Assistant Professor, Department of Mechanical Engineering, TKM College of Engineering, Kollam, Kerala, India.
[2]Professor, Department of Mechanical Engineering, TKM College of Engineering, Kollam. Kerala, India.

ABSTRACT - Prediction of BMD and Young's modulus of bones can highly enhance the scope for early detection and mitigation of untimely bone fracture and delay the associated difficulties that set in due to osteoporosis as one ages. It is demonstrated that microstructure and mechanical properties of bone can be derived from texture analysis of Computational Tomography (CT) images, using Gray Level Co-occurrence Matrix (GLCM) method. In the present work the authors attempted to establish a relationship between all the identified fourteen GLCM derived second order texture properties and bone mechanical properties. The fourteen textural features were acquired through GLCM matrix derived from QCT images of rabbit femur bone taken for the study. Method of Phantom calibration is implemented for computing bone mineral density (BMD). Bone mechanical properties like young's modulus and flexural rigidity are calculated from three-point bending test. The "Coefficient of Determination R^{2}" values for the correlation between each texture feature and the bone properties, such as Elastic Modulus, BMD and flexural modulus were computed. Out of the fourteen GLCM derived second order texture properties studied, energy, entropy, homogeneity, correlation and contrast showed significant relation with bone mechanical properties. Moreover, energy and entropy showed strong correlation with R square value greater than 0.6. The results show that the bone mechanical properties namely, BMD and young modulus can be predicted from second order textural features that are extracted from clinical image taken for any other diagnostic purpose. This can help clinicians for the early detection of osteoporosis, which aids in the prevention of medical emergencies arising from osteoporosis and can reduce the modulus mismatch during implantation which will result in best patient outcomes.

Keywords - Bone mechanical properties, Computed Tomography, Osteoporosis, Texture properties, GLCM,

1 INTRODUCTION

Bones play a vital role in keeping our body healthy. Bones undergo changes continuously; wherein new bone tissues are made and the old ones are broken down. According to Wolff's law, the mechanical properties might vary as bone is constantly remodelling and adapting to external load [1][2]. In adult the bone formation rate is higher than degeneration. As aging progress the bone formation rate decreases as compared to deformation rate[3]. Bone loss in aging due to high rate of bone deformation result in osteoporosis, if early detected and treated reduces the osteoporotic fracture. Osteoporotic fracture is the major concern for health care of elderly population.

Osteoporosis is a progressive, systemic, skeletal disorder which is characterized by low bone mass and deterioration of bone tissue in micro-architectural level, leads to increased bone fragility and fracture risk[4].The peak bone mass at young adulthood depends largely on genetic, biological and lifestyle factors, since low bone strength during the growing years is evidently associated with increased fragility fracture risk during old age[5].84% of osteoporotic fracture cases are due to ignorance of worsening of bone mass[6]. Detection of diminished quality of bone is critical in the prevention of osteoporotic fracture and helps in starting timely bone modulating therapies. Bone Mineral Density (BMD) plays a major role in evaluating the osteoporotic condition of a patient. Adults who are subjected to implantation leads to early osteoporotic condition due to modulus mismatch between host bone and implants. The implant fixation, accelerates bone degradation and failure due to stress shielding. The post-surgical problem like non-union or pseudarthrosis (possibly the result of stress shielding) and strut subsidence (possibly the result of a stiffer strut placed against a less stiff recipient bone) are due to modulus mismatches between host bone and implants[7]. Moreover, the moduli mismatch leads to excessive micro-motion between implants and bone, which inhibits bone formation and promotes fibrous tissue ingrowth, thereby preventing the osseointegration of the implant. Hence knowing the bone stiffness during implantation is necessary to reduce the large margin of stiffness between host bone and implant.

In vivo assessment of BMD and Bone stiffness (young's modulus) helps to minimise the fracture risk of osteoporotic condition. Many researchers have demonstrated that microstructure and mechanical properties of bone can be derived from texture analysis of Computational Tomography (CT) images, using Gray Level Co-occurrence Matrix (GLCM)method. Studies evaluated that the first and second order texture propertied are used for the classification of images[8].This method has been applied to various field like geoscience and remote sensing fields such as SAR sea ice, desert , cloud and soil [7][8][9] [10]. Haralick showed that the popular way of extracting second order texture features of the image is from the Gray level co-occurrence matrix (GLCM), which is a matrix with number of rows and columns is equal to the number of gray levels, G, in the image[11].

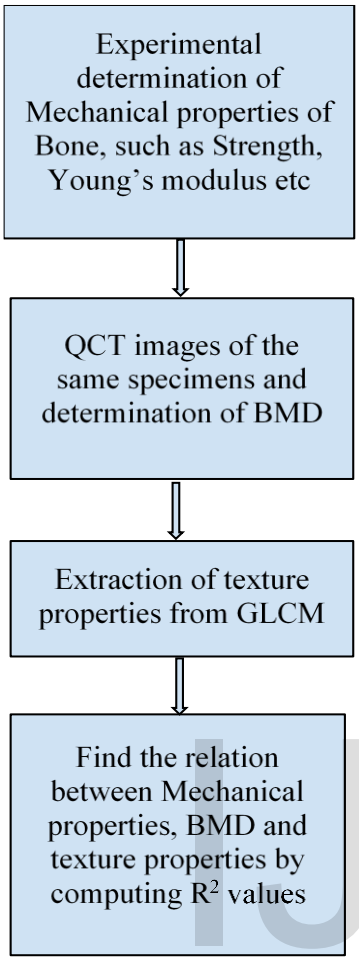

Figure [1] Methodology flow chart

It is reported that, fourteen textural features can be measured from the probability matrix(GLCM) to extract the texture characteristics of medical images[11].Studies reported that some GLCM texture properties like energy, contrast, entropy, autocorrelation, correlation, inverse difference moment, Cluster Shade have been evaluated from 2D projection image of bone and correlated with its BMD, Young's modulus and Bone volume fraction[7]. It is also reported that the GLCM feature 'correlation', outperformed energy, contrast, entropy, homogeneity and other GLCM features with a root-mean-square error metric used for predicting the trabecular BMD[8]. None of these studies compared the correlation performance of all fourteen GLCM parameters with the mechanical properties of bone.

In the present study, authors attempted to correlate all textural properties defined by Haralick[12] with the mechanical properties of bone which is obtained from mechanical testing of rabbit femur bone.

2 MATERIALS AND METHODS

Figure-1shows the flow chart of the present work for correlating second order image properties derived from QCT scan and the mechanical properties from three-point bending test of rabbit bone. The work consists of three stages. First, QCT image acquisition using GE optima QCT scanner having a calibration phantom- Catphan is performed. Secondly, the GLCM matrix from DICOM images are used for deriving second order texture properties defined by Haralick [12]. Finally, mechanical properties are calculated from a three-point bending test conducted on rabbit femur bone and bone mineral density is computed from QCT image of the same specimen. Following sections discusses the stepwise procedure of sample preparation and data acquisition from experiments conducted on rabbit femur bone.

Femur bone specimens of adult rabbit weighing approximately 1.75 - 2.5 kg are used for this study. Published methods for storage and handling of bone specimens were strictly followed during this investigation[13]. The specimens were kept at -20^{0}C in saline solution until tested.

Figure [2] The rabbit femur bone specimen sample

Figure [3] Rabbit femur bone in three-point bending test setup

They are thawed and kept moist with saline soaked sponge at room temperature, while preparing for Quantitative CT and experimentation. Ethics approval was obtained from the University ethics committee IAEC 1-KU-14/2019-20-TKM-PND (1). The specimen samples are shown in Figure [2] Mechanical test was conducted on table top UTM, INSTRON 3345, with Software BLUE HILL-3 at Sree Chitra Thirunal Institute for Medical Sciences and Technology, Trivandrum, An Institution of national importance under the Department of Science and Technology, Govt. of India. Each specimen was placed on the jig as shown in Figure [3] and gauge length was set to 30 mm. Knife-edge indenter of 4 mm in tip radius was used within the three-point bending test. Elastic bending test was carried out at a crosshead speed of 5 mm/min at 24^0C. Elastic modulus for each specimen was calculated using equation (1).

$$E = \frac{F}{\Delta}\left(\frac{L^3}{48I}\right) \quad \text{..... (1)}$$

Where E=young's Modulus, $\frac{F}{\Delta}$ =Slope of load - displacement graph, I= Moment of inertia, L=Gauge length (30mm). Flexural Strength of bone specimen was recorded during three-point bending test.

Bone Mineral Density of rabbit femur bone specimen was computed from the selected region of interest of CT image using calibration phantom. Figure-4 shows the sample DICOM/CT image of rabbit bone. Fifteen Rabbit femur bone specimens were prepared as per the procedure reported[14] and was subjected to QCT scanning (120kV-347mA, 0.625 mm slice thickness). A dedicated calibration phantom was placed in the scanner mat beneath the specimen. The QCT images obtained are analysed for identifying bone tissues or Region of interest (ROI) by calculating tissue distribution from the mean grey value or Hounsfield (HU) value. This is done by using a ROI tool in the software Sante-DICOM viewer. The selected region of interest of an image is saved as a jpeg image

Pixel attenuations (Hounsfield units or HU) on selected region of interest of CT images were converted to BMD values using a reference Catphan calibration phantom. The measured HU of the phantom and their corresponding equivalent densities are used to estimate slope and intercept parameters in equation (2), i.e., 'a' and 'b' of a linear model for converting HU values to BMD within a specified ROI. The HU values of these reference phantom rod and their known densities are used to construct a linear model, i.e.

Figure [4] Sample of ROI selected on DICOM image

$\rho = a + b\,HU$…… (2)
where, a=1.56 and b=0.00043
The second order texture features give information about the relative positions of the various gray levels within the image. The occurrence of some gray-level configuration can be described by a matrix of relative frequencies $P_{\theta, d}$ (L1, L2). It describes how frequently two pixels with gray-levels L1, L2 appear in the window separated by a distance d in direction θ. The information can be extracted from the co-occurrence matrix that measures second-order image statistics [15]. The co-occurrence matrix is a function of two parameters: relative distance measured in pixel numbers (d) and their relative orientation θ. The orientation θ is quantized in four directions that represent horizontal, diagonal, vertical and anti-diagonal by 0˚, 45˚, 90˚ and 135˚ respectively. Textural features which are derived from the co-occurrence matrix proposed by Haralick[12] are Angular Second Moment (ASM), Contrast, Correlation, Sum of Squares or Variance, Inverse Difference Moment, Sum Average, Sum Variance, Sum Entropy, Entropy, Difference Variance, Difference Entropy, Information Measure of Correlations and Cluster Tendency. The mathematical equations for computing the property values are listed in table appended (Appendix-A).

TABLE I
BONE MINERAL DENSITY OF RABBIT FEMUR BONE SAMPLES

Bone Sample	Bone Mineral Density (g/cm^3) (BMD)	Bone Sample	Bone Mineral Density (g/cm^3) (BMD)	Bone Sample	Bone Mineral Density (g/cm^3) (BMD)
1	1.675	6	1.947	11	1.891
2	1.795	7	1.809	12	1.876
3	1.751	8	1.917	13	1.76
4	1.701	9	1.801	14	1.873
5	1.734	10	1.783	15	1.876

The Haralick defined [12] second order texture parameters which quantify the spatial relationship between pixels in the area under investigation (ROI). The GLCM values with orientations 0^0, 45^0 and 90^0 for a displacement of one unit for the selected ROI unit were extracted from the QCT images of rabbit bone specimens. The texture parameters are computed from average GLCM values using MATLAB code.

TABLE II
YOUNGS MODULUS OF RABBIT FEMUR BONE SAMPLES

Bone Sample	Young's Modulus (E)(GPa)	Bone Sample	Young's Modulus (E)(GPa)	Bone Sample	Young's Modulus (E)(GPa)
1	2.40592	6	2.80716	11	1.99
2	2.63935	7	2.46376	12	2.23769
3	2.40849	8	2.684	13	2.3394
4	2.68061	9	1.76337	14	2.03775
5	1.94991	10	2.19208	15	2.42935

3 RESULTS AND DISCUSSIONS

In the present study, fifteen rabbit femur bone specimens were used for experimentation and imaging. The properties such as Elastic Modulus, Flexural Modulus and ultimate strength were obtained from three-point bending tests. The Bone mineral density was extracted from QCT images of the bone specimen using calibration phantom. The GLCM

values with orientations 0^0, 45^0 and 90^0 for a displacement of one unit were extracted from the QCT images of bone

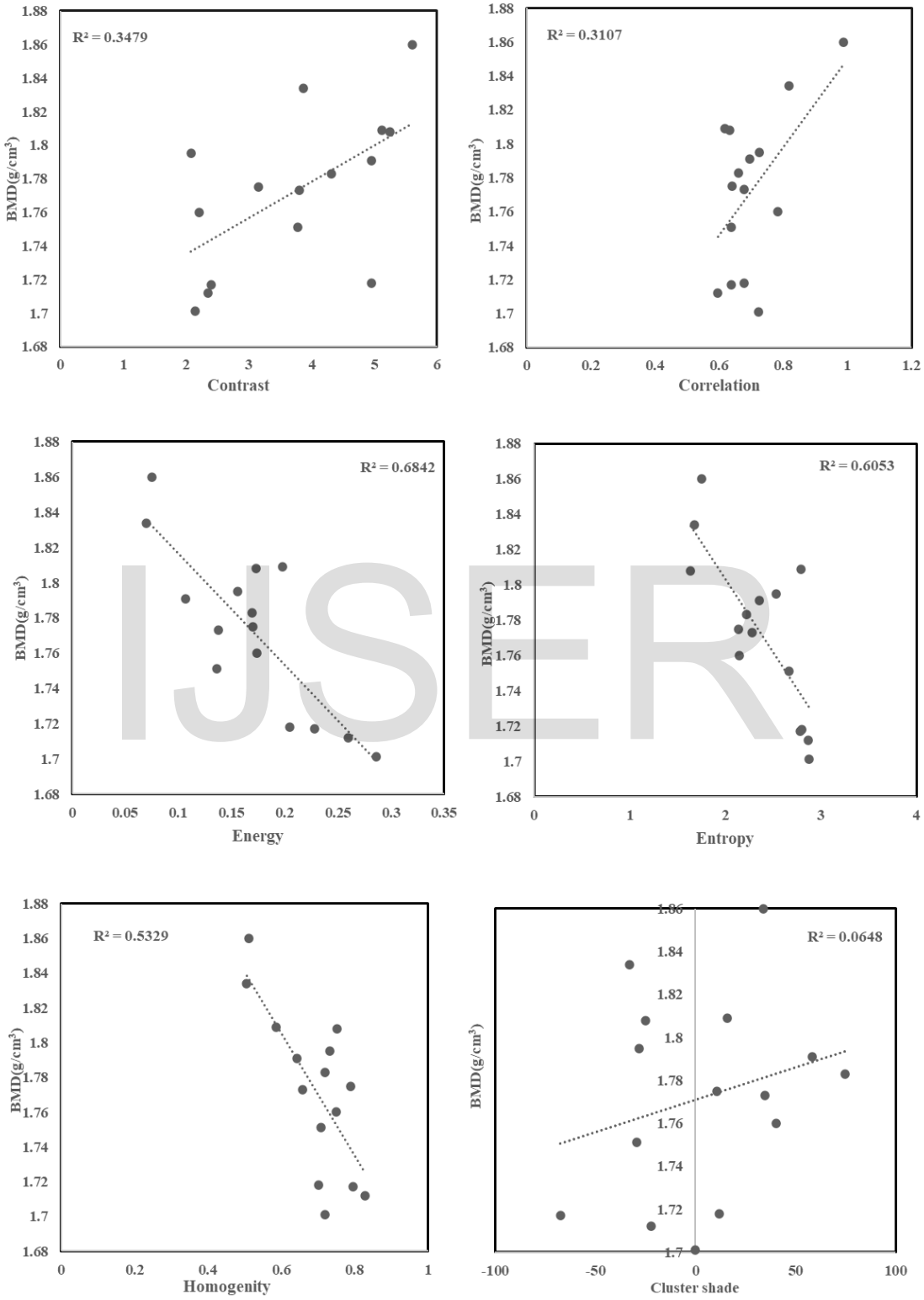

Figure [5] sample graphs showing correlation between Bone Mineral Density (BMD) of rabbit femur bone and second order texture properties computed from QCT image of the specimen.

specimens. The relationship of mechanical properties of bone such as Elastic Modulus, Flexural Modulus and Bone

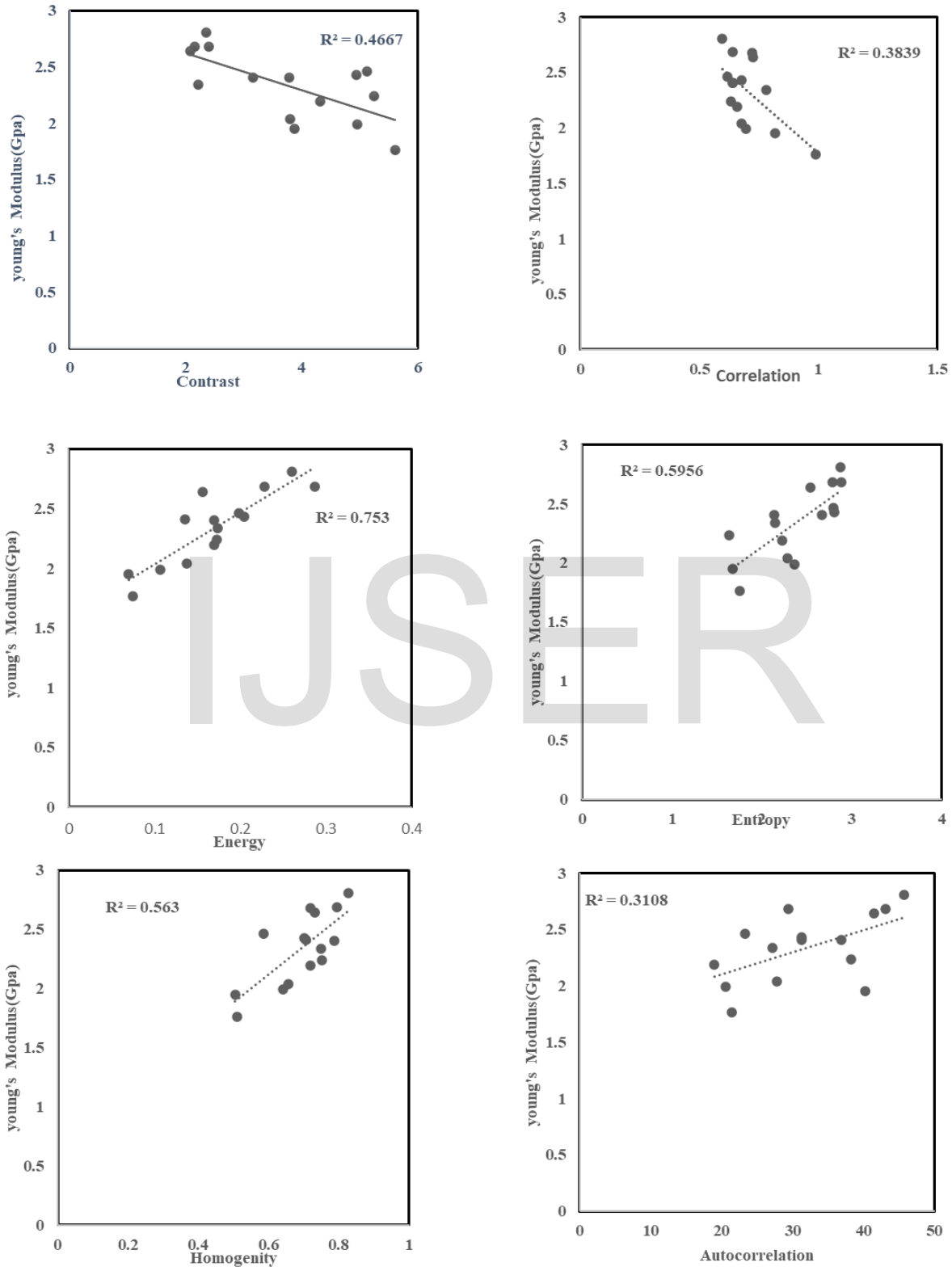

Figure [6] sample graphs showing correlation between Young's Modulus of rabbit femur bone and second order texture properties computed from QCT image of the specimen.

mineral density with the texture features computed from averaged GLCM, were determined statistically. The

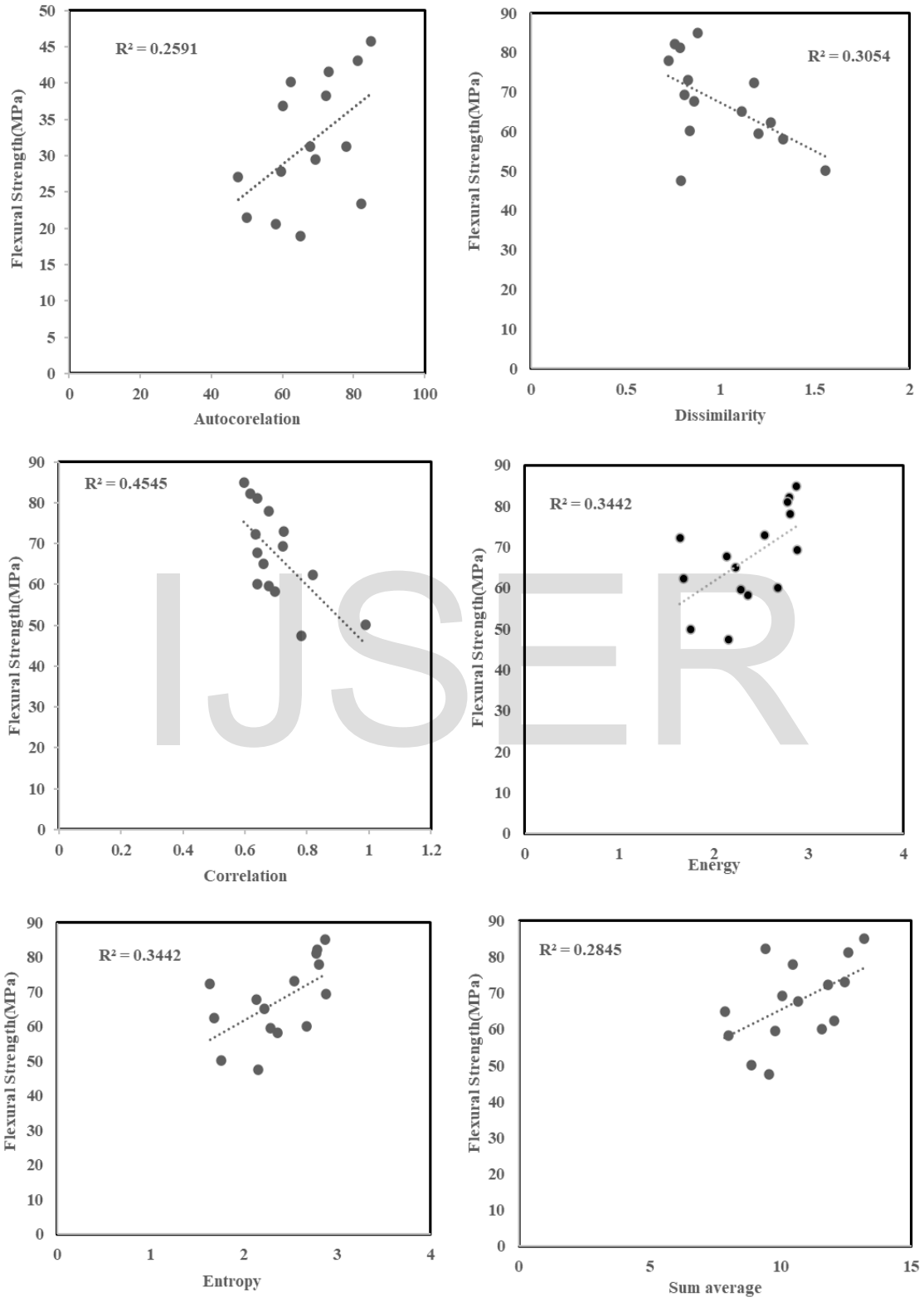

Figure [7] sample graphs showing correlation between Flexural Strength of rabbit femur bone and second order texture properties computed from QCT image of the specimen

"Coefficient of Determination R^2" values for the correlation between each texture feature and the bone properties, such as Elastic Modulus, Bone mineral density and flexural modulus were computed.

The BMD computed from QCT image using Calibration Phantom material is shown in table [1] Young's modulus was calculated from a load-displacement graph obtained during the three-point bending test on rabbit femur bone. The table [2] shows the computed value of Youngs Modulus

The multiple linear regression analysis conducted in this work revealed that out of the bone properties correlation of Elastic Modulus, Flexural Modulus, and Bone mineral density are in good agreement with the feature parameters extracted from GLCM. BMD shows a significant correlation with the five GLCM feature parameters such as entropy (r^2 =0.605) energy (r^2 =0.6842), correlation (r^2 =0.3107), homogeneity (r^2 =0.5329) contrast (r^2 =0.3479). It is noted that the Elastic modulus of bone showed correlation with texture properties such as entropy (r^2=0.5956), energy (r^2=0.753), homogeneity (r^2=0.563), contrast (r^2=0.4667) and correlation (r^2=0.38). The GLCM feature parameters like correlation, entropy, energy, dissimilarity, autocorrelation, sum average, sum variance shows R square values such as 0.4545,0.344,0.344,0.305,0.2591,0.28,0.26 respectively with Flexural Strength. The Figures [5][6][7] show the sample correlation graph of the above-mentioned properties with bone mechanical properties (Bone Mineral Density, Young's Modulus, Flexural Strength). Based on Multi-regression analysis for Haralick defined fourteen textural features with mechanical data of rabbit femur bone samples, it can be seen that texture properties such as entropy, energy, homogeneity, contrast and correlation show significant R square value with bone features. Among them energy and entropy show the best correlation with bone features. Hence, it can be concluded that, the above GLCM features parameter can be used as input parameters for predicting bone mineral density, flexural Modulus and Elastic modulus of bone.

4 CONCLUSIONS

In the present work the authors attempted to establish a relationship between GLCM derived second order texture properties and bone mechanical properties. The results presented in this work concluded that statistically correlated texture features such as entropy, energy, homogeneity, contrast and correlation computed from Gray Level Co-occurrence Matrices derived from bone images, shows significant correlation with bone mineral density and Young's Modulus. The GLCM feature parameters like correlation, entropy, energy, dissimilarity, autocorrelation, sum average, sum variance shows moderate correlation with flexural strength. Among the five significant properties energy and entropy show strong correlation with R square value greater than 0.6 with BMD and Young's Modulus. Hence the bone mineral density and young modulus values can be predicted by using the second order texture features extracted from clinical image taken for any diagnostic purposes.

Bone mineral density prediction from second order image properties using GLCM parameters helps clinicians for the early detection of osteoporosis, which aids in the prevention of medical emergencies arising from osteoporosis. The young's modulus prediction from texture features reduces the modulus mismatch during implantation and results in best patient outcomes.

Appendix A

Textural Features	Expression	Notation	Definition
Autocorrelation	$\sum_{i=1}^{N}\sum_{j=1}^{N}(i,j)p(i,j)$	X(i,j)	Elements i,j in the GLCM
Cluster prominence	$\sum_{i=1}^{N}\sum_{j=1}^{N}(i+j-2\mu)^3\ p(i,j)$	N	Number of gray-levels
Cluster Shade	$\sum_{i=1}^{N}\sum_{j=1}^{N}(i+j-2\mu)^4 p(i,j)$	P(i,j)	$\frac{x(i,j)}{\sum_{i=1}^{N}\sum_{j=1}^{N}x(i,j)}$
Contrast	$\sum_{i=1}^{N}\sum_{j=1}^{N}(i-j)^2\ p(i,j)$	p_x (i)	$\sum_{j=1}^{N}p(i,j)$
Correlation	$\sum_{i=1}^{N}\sum_{j=1}^{N}(\frac{i-\mu_x}{\sigma_x})(\frac{j-\mu_y}{\sigma_y})\ p(i,j)$	P_y (j)	$\sum_{i=1}^{N}p(i,j)$
Difference Entropy	$-\sum_{k=0}^{N-1}P_{x-y}(k)logP_{x-y}\ (k)$	μ_x	$\sum_{i=1}^{N}i.p_x$ (i)

Difference Variance	$\sum_{k=0}^{N-1}(k-\mu_{x-y})^2\ P_{x-y}(k)$	μ_y	$\sum_{j=1}^{N} j.p_y(j)$
Dissimilarity	$\sum_{i=1}^{N}\sum_{j=1}^{N}\lvert i-j\rvert.P(i,j)$	${\sigma_x}^2$	$\sum_{i=1}^{N}(i-\mu_x)^2.p_x(i)$
Energy	$\sum_{i=1}^{N}\sum_{j=1}^{N}p(i,j)^2$	${\sigma_y}^2$	$\sum_{j=1}^{N}(i-\mu_y)^2.p_x(j)$
Entropy	$-\sum_{i=1}^{N}\sum_{j=1}^{N}p(i,j)logp(i,j)$	$p_{x+y}(k)$	$\sum_{i=1}^{N}\sum_{j=1}^{N}p(i,j)$ i+j=k
Homogeneity	$\sum_{i=1}^{N}\sum_{j=1}^{N}\frac{p(i,j)}{1+(i-j)^2}$	$P_{x-y}(k)$	$\sum_{i=1}^{N}\sum_{j=1}^{N}p(i,j)$ $\lvert i-j\rvert=k$
Information measure of correlation 1	$\frac{HXY-HXY1}{\max(HX,HY)}$	μ_{x+y}	$\sum_{k=2}^{2N}k.p_{x+y}(k)$
Information measure of correlation 2	$\sqrt{1-\exp[-2(HXY2-HXY)]}$	μ_{x-y}	$\sum_{k=0}^{N-1}k.p_{x-y}(k)$
Inverse difference	$\sum_{i=1}^{N}\sum_{j=1}^{N}\frac{p(i,j)}{1+\lvert i-j\rvert}$	HX	$-\sum_{i=1}^{N}p_x(i).log\ p_x(i)$
Maximum Probability	$max_{i,j}\ p(i,j)$	HY	$-\sum_{i=1}^{N}p_y(i).log\ p_y(i)$
Sum average	$\sum_{k=2}^{2N}kp_{x+y}(k)$	HXY	$-\sum_{i=1}^{N}\sum_{j=1}^{N}p(i,j).\log p(i,j)$
Sum entropy	$-\sum_{k=2}^{2N}p_{x+y}(k)logp_{x+y}(k)$	$HXY1$	$-\sum_{i=1}^{N}\sum_{j=1}^{N}p(i,j).\log[p_x(i).p_y(j)]$
Sum of square	$\sum_{i=1}^{N}\sum_{j=1}^{N}(i-\mu)^2p(i,j)$	$HXY2$	$-\sum_{i=1}^{N}\sum_{j=1}^{N}p_x(i).p_y(j).log[p_x(i).p_y(j)]$
Sum variance	$\sum_{k=2}^{2N}(k-\mu_{x+y})^2\ p_{x+y}(k)$	$(Q(i,j)$	$\sum_{k=1}^{N}\frac{p(i,k)p(j,k)}{p_x(i)p_y(k)}$
Maximal Correlation Coefficient	$\sqrt{\lambda_2(Q(i,j))}$		

ACKNOWLEDGMENT

The authors would like to acknowledge the financial support from Research Seed money Scheme of TEQIP-II, TKM College of Engineering, Kerala, India and the support rendered by the Department of Medical Devices Engineering, Sree Chitra Tirunal Institute for Medical Sciences and Technology Devices Engineering, Trivandrum for conducting the experiment.

CONFLICTS OF INTEREST

The author(s) declare that they have no conflicts of interest with respect to the research, authorship, and/or publication of this article.

REFERENCES

[1] J.T. Stock, Wolff's law (bone functional adaptation), Int. Encycl. Biol. Anthropol. (2018) 1–2. https://doi.org/10.1002/9781118584538.ieba0521

[2] E. Seeman, Bone Modeling and Remodeling, Crit. Rev. Eukaryot. Gene Expr. 19 (2009) 219–233.

[3] D.J. Hunter, P.N. Sambrook, Bone loss: Epidemiology of bone

loss, Arthritis Res. 2 (2000) 441–445. https://doi.org/10.1186/ar125.

[4] WHO, Assessment of fracture risk and its application to screening for postmenopausal osteoporosis, 1994. https://doi.org/10.1109/TIP.2010.2050107.

[5] K.F. Janz, 2016 the year that was: Bone strength, Pediatr. Exerc. Sci. 29 (2017) 23–25. https://doi.org/10.1123/pes.2016-0279.

[6] J.F. Nishijima, Daniel; K. Simel, David L; Wisner, David H; Holmes, Bone mechanical properties and changes with osteoporosis, Physiol. Behav. 176 (2016) 139–148. https://doi.org/10.1016/j.physbeh.2017.03.040.

[7] R.F. Heary, N. Parvathreddy, S. Sampath, N. Agarwal, Elastic modulus in the selection of interbody implants, J. Spine Surg. 3 (2017) 163–167. https://doi.org/10.21037/jss.2017.05.01.

[8] Mukul Shirvaikar; Ning Huanga; XuanliangNeil Dongb;, THE MEASUREMENT OF BONE QUALITY USING GRAY LEVEL CO-OCCURRENCE MATRIX TEXTURAL FEATURES, Physiol. Behav. 176 (2018) 139–148. https://doi.org/10.1016/j.physbeh.2017.03.040.

[9] E. Ebert, Pattern Analysis Technique for Distinguishing Surface and Cloud Types in the Polar Regions., J. Clim. Appl. Meteorol. (1987) 1421–1426.

[10] Q.A. Holmes, D.R. Nuesch, R.A. Shuchman, Textural Analysis and Real-Time Classification of Sea-Ice Types Using Digital SAR Data, IEEE Trans. Geosci. Remote Sens. GE-22 (1984) 113–120. https://doi.org/10.1109/TGRS.1984.350602.

[11] T. Löfstedt, P. Brynolfsson, T. Asklund, T. Nyholm, A. Garpebring, Gray-level invariant Haralick texture features, PLoS One. 14 (2019) 1–18. https://doi.org/10.1371/journal.pone.0212110.

[12] A. Haralick, Robert M., Shanmugam. K, I. Dinstein, TexturalFeatures, IEEE Trans. Syst. Man Cybern. SMC-3, No. (1973) 610–621.

[13] M. Franklyn, B. Field, Experimental and finite element analysis of tibial stress fractures using a rabbit model, World J. Orthop. 4 (2013) 267–278. https://doi.org/10.5312/wjo.v4.i4.267.

[14] G.V.V. Wase U. Ahmed, Specimen Preparation of Bones , Tissues and, Buehler. 3 (1999).

[15] N. Aggarwal, R. K. Agrawal, First and Second Order Statistics Features for Classification of Magnetic Resonance Brain Images, J. Signal Inf. Process. 03 (2012) 146–153. https://doi.org/10.4236/jsip.2012.32019.

Appendix A			
Textural Features	Expression	Notation	Definition
Autocorrelation	$\sum_{i=1}^{N}\sum_{j=1}^{N}(i,j)p(i,j)$	X(i,j)	Elements i,j in the GLCM
Cluster prominence	$\sum_{i=1}^{N}\sum_{j=1}^{N}(i+j-2\mu)^3\ p(i,j)$	N	Number of gray-levels
Cluster Shade	$\sum_{i=1}^{N}\sum_{j=1}^{N}(i+j-2\mu)^4 p(i,j)$	P(i,j)	$\frac{x(i,j)}{\sum_{i=1}^{N}\sum_{j=1}^{N}x(i,j)}$
Contrast	$\sum_{i=1}^{N}\sum_{j=1}^{N}(i-j)^2\,p(i,j)$	p_x (i)	$\sum_{J=1}^{N}p(i,j)$
Correlation	$\sum_{i=1}^{N}\sum_{j=1}^{N}(\frac{i-\mu_x}{\sigma_x})(\frac{j-\mu_y}{\sigma_y})\,p(i,j)$	P_y (j)	$\sum_{i=1}^{N}p(i,j)$
Difference Entropy	$-\sum_{k=0}^{N-1}P_{x-y}(k)logP_{x-y}\ (k)$	μ_x	$\sum_{i=1}^{N}i.p_x\ (i)$
Difference Variance	$\sum_{k=0}^{N-1}\left(k-\mu_{x-y}\right)^2\ P_{x-y}(k)$	μ_y	$\sum_{j=1}^{N}j.p_y\,(j)$
Dissimilarity	$\sum_{i=1}^{N}\sum_{j=1}^{N}\lvert i-j\rvert.P(i,j)$	${\sigma_x}^2$	$\sum_{i=1}^{N}(i-\mu_x)^2.p_x(i)$
Energy	$\sum_{i=1}^{N}\sum_{j=1}^{N}p(i,j)^2$	${\sigma_y}^2$	$\sum_{j=1}^{N}\left(i-\mu_y\right)^2.p_x(j)$
Entropy	$-\sum_{i=1}^{N}\sum_{j=1}^{N}p(i,j)logp(i,j)$	$p_{x+y}(k)$	$\sum_{i=1}^{N}\sum_{j=1}^{N}p(i,j)$ i+j=k
Homogeneity	$\sum_{i=1}^{N}\sum_{j=1}^{N}\frac{p(i,j)}{1+(i-j)^2}$	$P_{x-y}(k)$	$\sum_{i=1}^{N}\sum_{j=1}^{N}p(i,j)$ $\lvert i-j\rvert=k$
Information measure of correlation 1	$\frac{HXY-HXY1}{\max(HX,HY)}$	μ_{x+y}	$\sum_{k=2}^{2N}k.p_{x+y}(k)$
Information measure of correlation 2	$\sqrt{1-\exp[-2(HXY2-HXY)]}$	μ_{x-y}	$\sum_{k=0}^{N-1}k.p_{x-y}(k)$
Inverse difference	$\sum_{i=1}^{N}\sum_{j=1}^{N}\frac{p(i,j)}{1+\lvert i-j\rvert}$	HX	$-\sum_{i=1}^{N}p_x\,(i).log\ p_x(i)$
Maximum Probability	$max_{i,j}\ p(i,j)$	HY	$-\sum_{i=1}^{N}p_y\,(i).log\ p_y(i)$
Sum average	$\sum_{k=2}^{2N}kp_{x+y}(k)$	HXY	$-\sum_{i=1}^{N}\sum_{j=1}^{N}p(i,j)\,.\log p(i,j)$
Sum entropy	$-\sum_{k=2}^{2N}p_{x+y}\,(k)logp_{x+y}(k)$	$HXY1$	$-\sum_{i=1}^{N}\sum_{j=1}^{N}p(i,j)\,.\log\left[p_x(i).p_y(j)\right]$
Sum of square	$\sum_{i=1}^{N}\sum_{j=1}^{N}(i-\mu)^2p(i,j)$	$HXY2$	$-\sum_{i=1}^{N}\sum_{j=1}^{N}p_x(i).p_y\,(j).log\left[p_x(i).p_y(j)\right]$
Sum variance	$\sum_{k=2}^{2N}(k-\mu_{x+y})^2\ p_{x+y}(k)$	$(Q(i,j)$	$\sum_{k=1}^{N}\frac{p(i,k)p(j,k)}{p_x(i)p_y(k)}$
Maximal Correlation Coefficient	$\sqrt{\lambda_2(Q(i,j))}$		